How Overconfident are Current Projections of Anthropogenic Carbon Dioxide Emissions?

Xihao Deng[1], Louis I. Miltich[2], Alexander Robinson[3], Richard S. J. Tol[4], Klaus Keller[5, 6, 7, *]

1 Department of Physics, Pennsylvania State University, University Park, Pennsylvania, United States of America
2 Department of Geoscience, Pennsylvania State University, University Park, Pennsylvania, United States of America
3 Department of Geoscience, Pennsylvania State University, University Park, Pennsylvania, United States of America
4 Department of Economics, University of Sussex, Falmer, East Sussex, England, United Kingdom
5 Department of Geoscience, Pennsylvania State University, University Park, Pennsylvania, United States of America
6 Earth and Environmental Systems Institute, Pennsylvania State University, University Park, Pennsylvania, United States of America
7 Department of Engineering and Public Policy, Carnegie Mellon University, Pittsburgh, Pennsylvania, United States of America
*** E-mail: kzk10@psu.edu**

Abstract

The longer-term risks of anthropogenic climate change hinges on sound probabilistic projections of CO_2 emissions. Previous projections have broken important new ground, but many provide only implicit probabilistic information. Here we take a step towards resolving this problem by assimilating globally aggregated observations of population size, economic output, and CO_2 emissions over the last three centuries into a simple economic model. We use this model to **derive probabilistic projections** of business-as-usual (BAU) CO_2 emissions to the year 2150. We demonstrate that the range of **several CO_2 emission scenarios** (e.g., from the BAUs of the DICE and FUND Models as well as Representative Concentration Pathways) misses potentially important tails of our projected probability density function. Studies that have interpreted the range of CO_2 emission scenarios as an approximation for the full forcing uncertainty may well be biased towards overconfident climate change projections.

Introduction

Anthropogenic carbon dioxide (CO_2) emissions cause climatic changes over many centuries [1]. Analyzing the risks associated with this anthropogenic perturbation requires sound probabilistic projections over the relevant timescale [2, 3]. Projections of anthropogenic climate forcing have broken important new ground [4, 5, 6, 7, 8, 9]. Yet, many projections still face potential problems due to (i) a lack of explicit and (ii) **potential overconfidence**.

One prominent approach to explore possible future CO_2 emissions is to derive scenarios that "cover a wide spectrum of alternative futures to reflect relevant

uncertainties" without explicitly assigning probabilities to different scenarios [10]. Such scenarios can be useful for exploratory modeling [11]. However, the lack of probabilistic information can leave scenario users guessing [12]. Furthermore, reporting a range of "plausible" scenarios [10] involves an implicit (but rather opaque) probabilistic statement. Probabilistic information is central to analyzing the risk trade-offs posed by climate change [2, 3, 13, 14, 15, 16].

Second, projections of CO_2 emissions used in scientific assessment may suffer from overconfidence. Overconfidence (i.e., estimating overly tight confidence bounds) is common in laboratory studies and scientific assessments [17, 18]. One indication of overconfidence in emission scenarios is the widening of the range of CO_2 emissions projected in 2100 as the prorated time approaches [5, 10]. This widening is an indicator of overconfidence because an unbiased error estimate shrinks **with** information. An additional indication of potential overconfidence in CO_2 emission scenarios is that they miss the tails of probabilistic projections [5]. Overconfidence in emission scenarios can bias risk analyses as they may underestimate the odds of low-probability high impact events [19, 20].

Here we take a step towards data-driven and coupled probabilistic projections of population size, economic output, and fossil fuel CO_2 emissions that extend beyond the 21st century. We use a Bayesian data assimilation framework to combine prior information with observational constraints. This hindcasting has proven to be a useful (but certainly not sufficient) test to identify structural model weaknesses and to estimate model parameters [2, 21]. We then use this model to derive an internally consistent BAU emissions projection to the year 2150. The Bayesian framework provides a rigorous and transparent way to derive probabilistic projections from a set of observations, structural assumptions, and clearly specified prior information. We use this framework to address three main questions: (i) What is the skill of a simple, mechanistic model in hindcasting the coupled system over several centuries? (ii) How realistic is the assumption that the emission scenarios of the Dynamic Integrated Climate-Economy (DICE) model [22], the Climate Framework for Uncertainty, Negotiation and Distribution (FUND) model [23] and the "Representative Concentration Pathways" (RCPs) [24] are a reasonable approximation for the range of relevant outcomes? (iii) What CO_2 emission projections beyond 2100 are consistent with a simple model and with key observational constraints?

Our study expands on several pioneering studies deriving probabilistic CO_2 emission projections. For example, Nordhaus and Yohe [2] assess projection errors by an out-of-sample backcast on a century timescale but do not perform a formal data assimilation. Pizer [25] assimilates observations to estimate a subset of model parameters using decadal timescale observation. Nordhaus and Yohe [2] as well as Pizer [25] use simple and globally aggregate models. In contrast, Reilly *et al.* [4] and Webster *et al.* [9] use more complex models, but **do not assimilate observational constraints**. Our study is intended as a proof of concept to demonstrate the feasibility of estimating all model parameters by assimilating century timescale observations. Our analysis captures the dynamics of population, economic output, and CO_2 emissions over the past three centuries reasonably well. The range of the DICE, FUND and RCP emission scenarios misses a sizable fraction of the tail-areas of our projected CO_2 emissions in 2100.

Our conclusions are subject to many caveats (discussed in more detail in the section "caveats and research needs" below). First, we choose a very simple model structure. Choosing a model complexity involves a trade-off between approximating the considered process and approximating the uncertainty analysis. Our choice of a simple model enables a relatively careful uncertainty analysis. Second, the analysis of past CO_2 emissions implies that we are deriving only approximately BAU projections. A better

characterization of the projections might be a "continuation of past policies" projection [7]. The projections still seem a reasonable approximation to a BAU case as efforts to reduce CO_2 emissions to date have had only small effects relative to century-scale dynamics. Third, our projections are subject to deep uncertainties associated with the necessary long-range assumptions [26]. It is crucial to stress that our projections are nothing but extrapolations of past observations with a transition to deeply uncertain long-term constraints. These projections can, of course, not predict the timing of unresolved shocks or surprises [27].

Data

We assimilate globally aggregated observations spanning the years 1700 to 2013. We use estimates of population and economic output made by Bolt and van Zanden (2014) [28]. The unit of gross world product used in [28] is Geary-Khamis dollar (international dollar) at the year of 1990. We use this unit for GWP for the rest of the paper unless otherwise specified. CO_2 emissions due to fossil fuel burning, gas flaring, and cement manufacturing are taken from Boden et al. (2013) [29] and Le Quéré et al. (2014) [30]. We do not consider CO_2 emissions by land use changes. Annual observations of population and economic output span from 1950 to 2010. Prior to 1950, these observations have a much more sparse resolution. CO_2 emissions estimates are annually resolved for the years 1750-2013.

The model

We adopt a simple globally aggregate modeling approach typical of many top-down integrated assessment models [31]. The model is composed of three coupled modules describing (i) population size, (ii) economic output, and (iii) anthropogenic CO_2 emissions. The unit of time in this model is one year.

Population

Following previous work, we model population growth by a logistic growth [32, 33], modified by an income sensitive net growth rate. Population P at time t is determined by:

$$P_t = P_{t-1}\left[1 + \left(\varphi_1 \frac{y_{t-1}}{\varphi_2 + y_{t-1}}\right)\frac{\varphi_3 - P_{t-1}}{\varphi_3}\right], \quad (1)$$

where y is annual per-capita income; ϕ_1 is the annual population growth rate; ϕ_2 is a half-saturation parameter with respect to per-capita consumption; and ϕ_3 is a logistic carrying capacity. This model structure reflects possible interactions between per capita income and population growth. Note that Eq. (1) implies that population grows and then stabilizes. Other projections assume that the world population peaks and then decreases [34].

Economic output

To model gross world product, we use a Cobb-Douglas production function accompanied by a Solow-Swan model of economic growth. Total world production Q at time t is

$$Q_t = A_t L_t^{\lambda} K_t^{1-\lambda}, \quad (2)$$

where A is total factor productivity; L is labor force; K is capital stock and represents the elasticity of production with respect to labor.

Total production is divided between consumption and investment where all output in a given year is assumed to be either consumed or saved

$$Q_t = U_t + I_t = (1 - s)Q_t + sQ_t, \tag{3}$$

where U is consumption; I is investment; and s is the proportion of savings. From this relationship, per capita income y follows as

$$y_t = \frac{Q_t}{P_t}. \tag{4}$$

Growth in total factor productivity occurs exogenously according to the Solow-Swan type growth model. The dynamics of long-term technological change are deeply uncertain [35, 36]. Following [22], we allow for a saturation of total factor productivity

$$A_t = A_{t-1} + \alpha A_{t-1}\left[1 - \frac{A_{t-1}}{A_s}\right], \tag{5}$$

where α is a growth rate parameter for total factor productivity and A_s represents a saturation level of total factor productivity. Capital stock dynamics are governed by the balance between investment levels in the previous year and capital loss due to depreciation

$$K_t = \left[(1 - \delta)K_{t-1} + I_{t-1}\right], \tag{6}$$

with δ representing the capital depreciation rate.

Labor at time t is determined by

$$L_t = \pi P_t, \tag{7}$$

where π is the labor participation rate.

Labor is initialized via an initial population parameter P_0 . Capital is initialized using the steady state relationship

$$K_0 = \left(\frac{sA_0}{\delta}\right)^{1/\lambda} L_0. \tag{8}$$

A **is initialized as a parameter** A_0. This results in six economic model parameters to be determined by calibration: λ, s, A_0, A_t, α and δ.

Anthropogenic CO_2 emissions

We approximate the link between economic output and anthropogenic CO_2 emissions through fossil fuel burning and cement production by a time dependent carbon intensity of production. The carbon emissions C at time t are

$$C_t = Q_t\phi_t, \tag{9}$$

where ϕ_t represents the carbon intensity at time t. The carbon intensity is modeled as the weighted average of four broadly defined technologies

$$\phi_t = \sum_{i=1}^{4} \gamma_{i,t}\rho_i, \tag{10}$$

where $\gamma_{i,t}$ is the fraction of the economy invested in technology i with carbon intensity ρ_i. The time dynamics of $\gamma_{i,t}$ are approximated as logistic penetration curves

$$\gamma_{1,t} = 1 - \frac{1}{1 + e^{-\kappa(t-\tau_2)}}, \tag{11a}$$

$$\gamma_{2,t} = \frac{1}{1 + e^{-\kappa(t-\tau_2)}} - \frac{1}{1 + e^{-\kappa(t-\tau_3)}}, \tag{11b}$$

$$\gamma_{3,t} = \frac{1}{1 + e^{-\kappa(t-\tau_3)}} - \frac{1}{1 + e^{-\kappa(t-\tau_4)}}, \text{ and} \tag{11c}$$

$$\gamma_{4,t} = \frac{1}{1 + e^{-\kappa(t-\tau_4)}}, \tag{11d}$$

with κ representing the rate at which technologies penetrate and τ_j ($j \subset [1..4]$) representing the times when the technology has penetrated half of the market. Such simple penetration patterns may reasonably approximate observed dynamics [37, 38]. We set the carbon intensity of the first technology (ρ_1) to zero to mimic a situation with negligible fossil fuel emissions (e.g., a subsistence agriculture with predominant use of biomass energy). Humans did cause fairly small CO_2 emissions prior to 1700 [39], but these emissions were largely driven by land-use changes, an emission source we do not consider in our analysis. We estimate the carbon intensities of the second and third technologies from the observations with the constraint $\rho_2 \geq \rho_3$. This constraint represents the transition from a high carbon intensity technology (i.e., predominant use of high carbon intensity fuels, such as coal) to a lower carbon intensity technology (i.e., shifting from coal to oil and natural gas as well as a shift towards a more service intense economy). We set the carbon intensity of the fourth technology to zero to allow for a long-term transition to a zero carbon emissions economy. We represent the limited resource base of conventional fossil fuels by constraining the total available fossil fuels to 6000 Gigatons of carbon (Gt C) [40]. Obviously, the constraint due to limited fossil fuel resources is subject to considerable uncertainty. One key uncertain factor is the future role of nonconventional fossil fuels derived from methane hydrates [41, 42].

Model coupling

The population model affects the economic model by providing the labor force. The economic model affects the population model through the sensitivity of the net growth rate on per-capita consumption. Finally, the CO_2 emissions model is driven from the economic model through the economic output. The coupled model yields 17 model parameters (Table 1) that are determined by using a Bayesian framework.

Bayesian analysis

We use a Bayesian data assimilation approach to calibrate the model and to estimate the effects of parametric uncertainty on future projections. The Bayesian approach is an efficient and statistically consistent method to assimilate observations into a nonlinear model with prior information and to derive probabilistic projections [43]. The use of prior information is a transparent and parsimonious way to represent information exogenous to the analyzed observations. Consider, for example, the task of projecting population levels over several centuries. Extrapolating the current trends results in projections that are at odds with independent assessments of the overall carrying capacity [33, 34]. One approach to this problem would be to explicitly represent the calculations leading to the estimates of carrying capacities in the model. We choose a second, arguably more transparent approach by representing these estimates as a Bayesian prior constraint on a model parameter.

Bayes theorem [44] allows us to combine prior estimates with new information to yield a posterior estimate

$$p(\vec{\theta}|\vec{\mathrm{d}}) = \frac{\Lambda(\vec{\mathrm{d}}|\vec{\theta})q(\vec{\theta})}{\int \Lambda(\vec{\mathrm{d}}|\vec{\theta})q(\vec{\theta})\, d\vec{\theta}}, \tag{12}$$

where $(\vec{\theta}|\vec{\mathrm{d}})$ is the posterior probability of the parameter vector $\vec{\theta}$ given the observations $\vec{\mathrm{d}}$; $\Lambda(\vec{\mathrm{d}}|\vec{\theta})$ is the likelihood of the observations given the parameters; and $q(\vec{\theta})$ is the prior probability of the parameters. We use prior values from previous studies and our own assessments (cf. Table 1). The denominator is a normalization constant to normalize the integral of the posterior probability to unity.

Likelihood function

The Bayesian approach requires evaluating the likelihood of the observations given the model parameters (and, implicitly, the adopted model structure). For identically independently distributed (iid) residuals from a Gaussian distribution, the likelihood function is given by:

$$\Lambda(\vec{\mathrm{d}}|\vec{\theta}) = \prod_{k,i} \frac{1}{\sqrt{2\pi\sigma_k^2}} \exp\left[-\frac{1}{2}\left(\frac{f(\vec{\theta}, t_k^i) - \mathrm{d}_k^i}{\sigma_k}\right)^2\right]. \tag{13}$$

In this equation, the index k and i denote respectively the index of subject (e.g. population, GWP and CO_2 emission) and the index of the time; f denotes the model introduced in the previous section. To investigate the validity of the iid assumption, we use a differential evolution algorithm [45] to maximize the likelihood in Eq. (13) over the model parameter $\vec{\theta}$ to obtain the best-fit model; we then subtract the best-fit model from the observations to obtain the residuals and to see if the residuals are uncorrelated. The analysis shows that the iid assumption is violated for the model residuals for the annual population, economic output and CO_2 emissions as they show statistically significant autocorrelation, i.e., the residuals are very similar to a lagged version of themselves over successive time intervals (Figure 1, Figure 2 and Figure 3).

The amplitudes of the annual residuals increase with time (Figure 1, Figure 2 and Figure 3), i.e., they are heteroscedastic. This heteroscedasticity may be caused by the exponentially increasing long trend values of the population growth, economic output and CO_2 emission. We **represent this by assuming** the residuals of the log observations are homoscedastic first order autoregressive processes (AR), i.e.,

$$r_k^i = \log(\mathrm{d}_k^i) - \log(f(\vec{\theta}, t_k^i)) = a_k r_k^{i-1} + n_k^i\,, \tag{14}$$

where a_k is the AR coefficient and n_k^i is the AR error that is white Gaussian [46, chap. 3], because the residuals in percentage terms may be rather stable than varying [46, chap. 21]. Our analysis supports this assumption (see bottom-left panels of Figure 1, Figure 2 and Figure 3).

We follow [47] and modify the likelihood function for the annual observations to account for the autoregressive residuals. Following [25], we neglect potential correlations between the model residuals for the different observational constraints (e.g., between population size and CO_2 emissions). For non-annual data (sparse data of population and GWP observed prior to 1950), we neglect possible effects of autocorrelation and assume they are white Gaussian.

This approach results in eight parameters to characterize the residuals of the observations: one AR coefficient and one rms of AR error for each of the three annual data sets (population, GWP and CO_2); and two rms parameters for the non-annual

observations of population and GWP. To recap, we have totally 25 parameters to be determined — 17 parameters characterizing the long trend model introduced in the previous secion and 8 parameters characterizing the residuals.

Computation method

We use the Metropolis-Hastings algorithm [48, 49] to derive the posterior probability, the probabilistic hindcasts and projections. This Monte Carlo method allows us to account for the full nonlinear model behavior and to characterize the posterior probability without making parametric distribution assumptions. This algorithm constructs a Markov chain of parameter vectors that represent direct draws from the posterior probability. The algorithm samples efficiently from the posterior probability by probabilistically accepting a parameter vector into the chain based on the gradient of the likelihood function. Using the gradient information allows for preferential sampling in regions with high posterior likelihood. The probabilistic formulation of the acceptance rule minimizes the risk of getting trapped on a local maximum of the posterior probability.

The Markov chain starts from an initial parameter guess $\vec{\theta}_i$. The likelihood of this parameter vector is computed and compared to the likelihood of a candidate parameter vector $\vec{\theta}_c$ chosen by stepping a specified distance from the previous parameter vector in a direction chosen from a uniform proposal distribution. The candidate vector is accepted into the chain if

$$\frac{\Lambda(\vec{\mathrm{d}}|\vec{\theta}_c)q(\vec{\theta}_c)}{\Lambda(\vec{\mathrm{d}}|\vec{\theta}_i)q(\vec{\theta}_i)} > U, \tag{15}$$

where U is a uniform random variable between 0 and 1. This rule allows a higher probability of moving up gradient towards regions of high likelihood mass but also allows the possibility of moving down gradient. Allowing the algorithm to move down gradient as well as up reduces the risk of misconvergence to a local maximum of the posterior pdf. If a candidate point is accepted, the process is repeated with $\vec{\theta}_c$ replacing $\vec{\theta}_i$. The chain eventually retains no memory of the starting guess. After a sufficient "burn-in" period, which is removed from the analysis, the chain converges to a stationary sample from the posterior probability. We use simple heuristic rules to identify the necessary burn-in and chain lengths [50]. This procedure results in a final chain length of roughly 10^7 samples. Using 10 independent chains with different initial conditions resulted in **consistent estimates of** the posterior probability density function. We sample from this posterior probability to derive the hindcasts and projections. The model code, the analyzed data, and the assimilation algorithm are available **in Github**.

Results and discussion

In this section we discuss the hindcasts and projections made by our analysis, and we will also compare them with the BAU scenarios of the DICE model [22], the FUND model [23] and six RCPs [24].

The population hindcast captures the recent transition to decreasing growth rates [33] reasonably well (Figure 7, top panel). It projects that the population level starts to saturate in around 2100, and the mode of the saturation level is nine billion in 2100 (Figure 8, top-left panel). The BAU scenarios of the DICE model and the FUND model fall **at around 90% percentile** of our analysis (Figure 7, top panel).

The projected gross world product continues to grow (Figure 7, middle panel), but with a decreasing growth rate (Figure 8, top-middle panel). This decreasing growth rate of GWP is driven in this simple model by decreasing growth rates for population and

for total factor productivity, two key inputs to the production function. However, the posterior predictive distributions of GWP have heavy tails (Figure 8, top-middle panel), extending beyond about 400 trillion dollars per year with 1% probability. This large uncertainty level results from the large uncertainties of the posterior estimations of the capital deprecation rate, the rate of technological progress and other economic parameters (Figure 5). The BAU scenario of the FUND model falls at around 90% percentile of our analysis. However, that of the DICE model extends far beyond the 1% percentile after about 2050. One potential reason of this is the economic model used in DICE, which unlike our model, assumes the extensive techological progresses driving rapid GWP growth [22].

The CO_2 emission hindcast presents significant uncertainties after about 1950, which primarily results from the **strong residuals** (Figure 3). The median CO_2 emission projections show a peak of 15 Gigatons of carbon per year (Gt C/a) around 2100 with a subsequent slow decline (Figure 7, bottom panel). MAP estimate of CO_2 emission projections declines from 15 Gt C/a at 2050 to 3 Gt C/a at 2150. This projected reduction in emission is driven by the constraint on total available fossil fuel resources and the observed decrease in carbon intensity in the last few decades [22, 51]. However, the posterior predictive distributions of CO_2 emission have heavy tails, extending to 70 Gt C/a with 1% probability (Figure 8, top-right panel). This large uncertainty results from two aspects: (i) poor constraints of carbon intensities of different technologies and half-saturation time of the carbon clean technology (Figure 6); (ii) strong residuals of carbon emission caused by short term fluctuations of business cycles (Figure 3), which is unfortunately ignored by previous studies (e.g. [52]). BAU emission scenarios of the DICE model, the FUND model and the RCPs all fall within 70% percentile of our projection (Figure 7, bottom panel). The uncertainty level of our analysis is much wider than previous studies, which indicates our study forecasts considerably higher climate risk than previous analyses.

We analyze the potential biases caused by the subjective choice of prior distributions (Table 1). We change the prior distributions of some parameters and compare the projectins of the corresponding population, GWP and CO_2 emissions. The priors we change are:

(i) Population carrying capacity (φ_3): change from normal to uniform distribution with the same bounds.

(ii) Carbon intensity of technology 2 (ρ_2): change from uniform to log-normal distribution with shape parameter of 0.5 and log-scale of log(6), the 99% confidence interval of which covers from 0 to 0.5.

(iii) Half-saturation time of technology 4 (τ_4): remain uniform distribution but change the upper bound from 2500 to 2300.

The prior predictive distributions of population, GWP and CO_2 emission at 2050 have different skewnesses and kurtoses (Figure 8, bottom panel). However, the posterior predictive distributions converge to the same distributions (Figure 8). This indicates that our projections primarily depends on data-dependent likelihood function and are insensitive to the data-independent prior distributions.

Caveats and research needs

Our conclusions are subject to several caveats that point towards research needs. First, the model is a simple approximation that neglects likely important structural details. Potentially important structural refinements include dynamical representations of (i)

changes in the economic sectors [53], (ii) population carrying capacity [33], (iii) the savings rate [54], (iv) endogenous technological change [55], and (v) capital stock effects [56]. Furthermore, we aggregate observations to a global scale.

Second, our projections neglect potentially important structural uncertainties. Structural uncertainty is a key concern in models of socioeconomic systems [16, 57]. In our analysis, we consider only a small subset of structural uncertainties. A more complete consideration of structural uncertainties would widen the projection range [58]. As a result, our projections still suffer from overconfidence. A more complete consideration of structural uncertainty would, however, also strengthen our conclusion that the scenarios of previous studies, such as those of the DICE model, the FUND model and the RCPs, may be overconfident.

Conclusion

We assimilate observations of population size, economic output, and CO_2 emissions into a simple model to derive probabilistic hindcasts and projections on a century timescale. The 99% confidence range of our CO_2 emission projections extends considerably beyond the range covered by past CO_2 emission scenarios [22, 23, 24]. We incorporate the effects of the import short term fluctuations caused by business cycles into our analysis, which are unfortunately ignored by previous studies (e.g. [52]). These effects may widen the projection range.

Our results are consistent with the hypothesis that previous BAU emission scenarios are overconfident and cover only a subset of the potential future outcomes. An alternative hypothesis is that assimilating less aggregated observations into a structurally more complex model would result in a tighter projection range. Testing this alternative hypothesis is possible using our method, but would be beyond the scope of this proof of concept study.

Analyzing the risks of anthropogenic CO_2 emissions requires a careful assessment of the odds of different CO_2 emissions over the relevant multicentury timescale. Deriving these projections is a daunting (and so far open) challenge. We show that a Bayesian data assimilation in conjunction with a simple, transparent, and concise model can provide reasonable probabilistic hindcasts over the last three centuries. A quantitative understanding of the past dynamics is, of course, just a necessary condition for a skillful probabilistic projection of possible futures, but it is a start.

Acknowledgments

We thank Arnulf Grübler, Jonathan Koomey, Robert Lempert, Michael Obersteiner, Brian O'Neill, Hugh Pitcher, Steve Smith, Rob Socolow, Dan Ricciuto, and Mort Webster for helpful discussions. Mary Haight provided editorial assistance. This paper was conceived at an EMF Snowmass workshop, thanks to the wonderful environment created by Susan Sweeney and John Weyant. The Hamburg University Innovation Fund, the Princeton Environmental Institute, the Princeton Carbon Mitigation Initiative, **the National Science Foundation**, and the ESRI Energy Policy Research Centre provided welcome financial support. None but the authors are responsible for opinions and errors in this paper.

References

1. Archer D, Ganopolski A (2005) A movable trigger: Fossil fuel CO_2CO2 and the onset of the next glaciation. Geochem Geophys Geosyst 6: Q05003.

2. Nordhaus WD, Yohe GW (1983) Future carbon dioxide emissions from fossil fuels. In: Changing Climate: Report of the Carbon Dioxide Assessment Committee., National Research Council, Washington D.C, United State of America: National Academy Press.

3. Allen MR (2003) Possible or probable? Nature 425: 242.

4. Reilly JM, Edmonds JA, Gardner RH, Brenkert A (1987) Uncertainty analysis of the IEA/ORAU CO_2CO2 emissions model. Energ J 8: 1-29.

5. Leggett J, Pepper WJ, Swart RJ (1992) Emissions scenarios for the IPCC: An update. In: Houghton JT, et al., editors, Climate Change 1992: The Supplementary Report to the IPCC Scientific Assessment, Cambridge, United Kingdom: Cambridge University Press.

6. Nordhaus WD, Popp D (1997) What is the value of scientific knowledge? An application to global warming using the PRICE model. Energ J 18: 1-45.

7. Schmalensee R, Stoker TM, Judson RA (1998) World carbon dioxide emissions: 1950-2050. Rev Econ Stat 61: 15-27.

8. Nakicenovic N (2000) Greenhouse gas emissions scenarios. Technol Forecast Soc Change 65: 149-166.

9. Webster MD, Babiker M, Mayer M, Reilly JM, Harnisch J, et al. (2002) Uncertainty in emissions projections for climate models. Atmos Environ 36: 3659-3670.

10. Nakicenovic N, Alcamo J, Davis G, Vries BD, Fenhann J, et al. (2000) Special report on emissions scenario. Cambridge, United Kingdom: Cambridge University Press.

11. Bankes S (1993) Exploratory modeling for policy analysis. Oper Res 41: 435-449.

12. Wigley TML, Raper SCB (2001) Interpretation of high projections for global-mean warming. Science 293: 451-454.

13. Kann A, Weyant JP (2000) Approaches for performing uncertainty analysis in large scale energy/economic policy models. Environ Model Assess 5: 29-46.

14. Pittock AB, Jones RN, Mitchell CD (2001) Probabilities will help us plan for climate change: Without estimates, engineers and planners will have to delay decisions or take a gamble. Nature 413: 249.

15. Schneider SH (2002) Can we estimate the likelihood of climatic changes at 2100? Clim Change 52: 441-451.

16. Webster MD (2003) Communicating climate change uncertainty to policy-makers and the public: an editorial comment. Clim Change 61: 1-8.

17. Alpert M, Raiffa H (1982) A progress report on the training of probability assessors. In: Kahneman D, et al., editors, Judgment Under Uncertainty: Heuristics and Biases, Cambridge, United Kingdom: Cambridge University Press.

18. Henrion M, Fischhoff B (1986) Assessing uncertainty in physical constants. Am J Phys 54: 791-798.

19. Gregory JM, Dixon KW, Stouffer RJ, Weaver AJ, Driesschaert E, et al. (2005) A model intercomparison of changes in the Atlantic thermohaline circulation in response to increasing atmospheric CO_2CO2 concentration. Geophys Res Lett 32: 10143-10162.

20. Challenor PG, Hankin RKS, March R (2006) Towards the probability of rapid climate change. In: Schellnhuber HJ, editor, Avoiding dangerous climate change, Cambridge, United Kingdom: Cambridge University Press.

21. Hargreaves JC, Annan JD (2002) Assimilation of paleo-data in a simple Earth system model. Clim Dyn 19: 371-381.

22. Nordhaus WD (1994) Managing the global commons: The economics of climate change. Cambridge, Massachusetts, United State of America: The MIT Press.

23. Tol RSJ (2005) An emission intensity protocol for climate change: an application of FUND. Clim Policy 4: 269-287.

24. Moss RH, Edmonds JA, Hibbard KA, Manning MR, Rose SK, et al. (2010) The next generation of scenarios for climate change research and assessment. Nature 463: 747-756.

25. Pizer WA (1999) The optimal choice of climate change policy in the presence of uncertainty. Resour Energy Econ 21: 255-287.

26. Lempert R, Schlesinger ME (2001) Climate-change strategy needs to be robust. Nature 412: 375.

27. Craig PP, Gadgil A, Koomey JG (2002) What can history teach us? A retrospective examination of long-term energy forecasts for the united states. 27: 83-118.

28. Bolt J, van Zanden JL (2014) The Maddison Project: collaborative research on historical national accounts. Econ Hist Rev 67: 627-651.

29. Boden TA, Marland G, Andres RJ (2013) Global, regional, and national fossil-fuel CO_2CO2 emissions. In: Carbon Dioxide Information Analysis Center, Oak Ridge, Tennessee, United State of America: Oak Ridge National Laboratory, U.S. Department of Energy.

30. Quéré CL, Moriarty R, Andrew RM, Peters GP, Ciais P, et al. (2014) Global carbon budget 2014. Earth Syst Sci Data Discuss 7: 521-610.

31. Nordhaus WD, Boyer J (2000) Warming the world: Economic models of global warming. Cambridge, Massachusetts, United State of America: The MIT Press.

32. Verhulst PF (1838) Notice sur la loi que la population pursuit dans son accroissement. Correspondance mathématique et physique 10: 113-121.

33. Cohen JE (1995) Population growth and earth's human carrying-capacity. Science 269: 341-346.

34. Lutz W, Sanderson W, Scherbov S (2001) The end of world population growth. Nature 412: 543-545.

35. Starr C, Rudman R (1973) Parameters of technological growth. Science 182: 358-364.

36. Ausubel JH (1995) Technical progress and climatic-change. Energy Policy 23: 411-416.

37. Marchetti C (1977) Primary energy substitution models: Interaction between energy and society. Technol Forecast Soc Change 10: 345-356.

38. Grübler A, Nakicenovic N, Victor DC (1999) Dynamics of energy technologies and global change. Energy Policy 27: 247-280.

39. Ruddiman WF (2003) The anthropogenic greenhouse era began thousands of years ago. Clim Change 61: 261-293.

40. Rogner HH (1997) An assessment of world hydrocarbon resources. Annu Rev Energ Env 22: 217-262.

41. Milkov AV (2004) Global estimates of hydrate-bound gas in marine sediments: How much is really out there? Earth-Sci Rev 66: 183-197.

42. Klauda JB, Sandler SI (2005) Global distribution of methane hydrate in ocean sediment. Energy Fuels 19: 459-470.

43. Brand KP, Small MJ (1995) Updating uncertainty in an integrated risk assessment: conceptual framework and methods. Risk Anal 15: 719-731.

44. Bayes T (1763) An essay towards solving a problem in the doctrine of chances. Phil Trans 53: 371-418.

45. Storn R, Price K (1995). Differential evolution: a simple and efficient adaptive scheme for global optimization over continuous spaces.

46. Hamilton JD (1994) Time series analysis. Princeton, New Jersey, United State of America: Princeton University Press.

47. Zellner A, Tian GC (1964) Bayesian analysis of the regression model with autocorrelated errors. J Am Stat Assoc 59: 763-778.

48. Metroplis N, Rosenbluth AW, Rosenbluth MN, Teller AH, Teller E (1953) Equation of state calculations by fast computing machines. J Chem Phys 21: 1087-1092.

49. Hastings WK (1970) Monte-Carlo sampling methods using Markov chains and their applications. Biometrika 57: 97-109.

50. Raftery AE, Lewis SM The number of iterations, convergence diagnostics and generic Metropolis algorithms.

51. Grübler A, Nakicenovic N (1996) Decarbonizing the global energy system. Technol Forecast Soc Change 53: 97-110.

52. Dowlatabadi H, Oravetz MA (2006) Us long-term energy intensity: backcast and projection. Energy Policy 34: 3245-3256.

53. Kongsamut P, Rebelo S, Xie DY (2001) Beyond balanced growth. Rev Econ Stud 68: 869-882.

54. Deaton A, Paxson C (2000) Growth and saving among individuals and households. Rev Econ Stat 82: 212-225.

55. Romer D (1996) Advanced Microeconomics. New York City, New York, United State of America: McGraw Hill.

56. Edmonds J, Reilly J (1983) A long-term global energy-economic model of carbon-dioxide release from fossil-fuel use. Energ Econ 5: 74-88.

57. Koomey JG (2002) Avoiding "The Big Mistake" in forecasting technology adoption. Technol Forecast Soc Change 69: 511-518.

58. Draper D (1995) Assessment and propagation of model uncertainty. J R Stat Soc Series B Stat Methodol 57: 45-97.

59. Lutz W, Sanderson W, Scherbov S (1997) Doubling of world population unlikely. Nature 387: 803-805.

60. Maddison A (2004) The world economy: historical statistics. OECD.

61. Nadiri MI, Prucha IR (1996) Estimation of the depreciation rate of physical and R&D capital in the us total manufacturing sector. Econ Inq 34: 43-56.

62. Grübler A (1991) Diffusion: Long-term patterns and discontinuities. Technol Forecast Soc Change 39: 159-180.

63. Jeffreys H (1946) An invariant form for the prior probability in estimation problems. Proc R Soc London, Ser A 186: 453.

64. Uhlenbeck GE, Ornstein LS (1930) On the theory of brownian motion. Phys Rev 36: 823-841.

65. Juglar C (2010) Des Crises commerciales: et leur retour periodique en France, en Angleterre, et aux Etats-Unis. Paris, France: Kessinger Publishing, LLC.

Figure legends

Figure 1: Observations, best-fit model and residuals of the population growth. The left side presents the observations & best-fit model (top-left), residuals of annual data (middle-left), and AR errors of residuals of the annual log population growth (bottom-left). The right side presents probability density function (top-right), cumulative density function (middle-right) and quantile-quantile plot (bottom-right) of the AR errors. It shows that the residuals of the annual observations are heteroscedastic and autocorrelated, but the autoregressive errors of the residuals of the annual log data are approximately white Gaussian.

Figure 2: Observations, best-fit model and residuals of the gross world product. The left side presents the observations & best-fit model (top-left), residuals of annual data (middle-left), and AR errors of residuals of the annual log GWP (bottom-left). The right side presents probability density function (top-right), cumulative density function (middle-right) and quantile-quantile plot (bottom-right) of the AR errors. It shows that the residuals of the annual observations are heteroscedastic and autocorrelated, but the autoregressive errors of the residuals of the annual log data are white Gaussian.

Figure 3: Observations, best-fit model and residuals of the carbon emission. The left side presents the observations & best-fit model (top-left), residuals of annual data (middle-left), and AR errors of residuals of the annual log carbon emission (bottom-left). The right side presents probability density function (top-right), cumulative density function (middle-right) and quantile-quantile plot (bottom-right) of the AR errors. It shows that the residuals of the annual observations are heteroscedastic and autocorrelated, but the autoregressive errors of the residuals of the annual log data are white Gaussian.

Figure 4: Marginal posterior probability densities of parameters characterizing population growth, including those characterizing both the long trend model and the residuals. The blue solid line denotes posterior and the red dashed line denotes prior.

Figure 5: Marginal posterior probability densities of parameters characterizing gross world product, including those characterizing both the long trend model and the residuals. The blue solid line denotes posterior and the red dashed line denotes prior.

Figure 6: Marginal posterior probability densities of parameters characterizing carbon emission, including those characterizing both the long trend model and the residuals. The blue solid line denotes posterior and the red dashed line denotes prior.

Figure 7: Hindcasts and forecasts of population, gross world product and carbon emission from year 1700 to 2150, and their comparison with BAU scenarios of DICE model (dashed lines), FUND model (dot-dashed lines) and six RCPs (dot lines). The colorbar represents the percentiles of the corresponding posterior distributions and posterior predictive distributions. The 99% percentile range covers all the previous BAU scenarios, except the economic output projection of the DICE model. However, previous BAU scenarios miss important tails of our posterior predictive distributions.

Figure 8: Upper panel: marginal predictive posteriors of population, GWP and carbon emission Projections for the years 2050 (blue line), 2100 (red line) and 2150 (green line). The population level saturates at 9 billion after the year of 2050. The MAP

of the GWP gradually grows from about 100 trillion dollars per year at 2050 to about 300 trillion at 2150. The tail of the posterior distribution of the GWP becomes heavier over time. The MAP of the carbon emission decreases from about 15 G t/a to about 0 G t/a. However, the posterior distribution of the carbon emission becomes skewer and has a heavier tail over time. Lower panel: comparison of two different prior predictive distributions and two different posterior predictive distributions of population, GWP and carbon emission at 2050. The blue dash line and blue solid line respectively denote the predictive distributions of first prior and the corresponding posterior. The red dash line and red solid line respectively denote the predictive distributions of the second prior and the corresponding posterior. Although the prior predictive distributions are different for different prior distributions, the posterior predictive distributions converge to the same distributions.

Tables

Parameter	Description	Units	Prior	Lower bound	Upper bound	Reference
φ_1	population growth rate	1/year	uniform	0.0001	0.15	this study
φ_2	half-saturation constant	1,000 \$/ (year capita)	uniform	0	100	this study
φ_3	population carrying capacity	billions	normal	6.9	14.4	Lutz *et al.* [59][a]
φ_4	population in 1700	billions	normal	0.3	0.9	Maddison [60][b]
λ	elasticity of production with respect to labor	dimensionless	normal	0.6	0.8	Romer [55]
s	savings rate	dimensionless	normal	0.18	0.26	this study[c]
$\delta(< s)$	capital deprecation rate	1/year	uniform	0.01	0.14	Nordhaus [22] Nadiri & Prucha [61]
α	rate of technological progress	1/year	uniform	0.0007	0.0212	this study
A_s	saturation level of total factor productivity	dimensionless	uniform	5.3	16.11	Nordhaus [22][d]
π	labor participation rate	dimensionless	normal	0.51	0.67	this study
A_0	initial total factor productivity	dimensionless	uniform	0	3	this study[e]
ρ_2	carbon intensity of technology 2	kg carbon/ 1990 \$	uniform	0	0.5	this study
ρ_3	carbon intensity of technology 3	kg carbon/ 1990 \$	uniform	0	0.5	this study
τ_2	half-saturation time of technology 2	year	uniform	1700	2100	this study
τ_3	half-saturation time of technology 3	year	uniform	1700	2100	this study
τ_4	half-saturation time of technology 4	year	uniform	2010	2500	this study
κ	time constant of technological penetration	1/year	uniform	0.005	0.2	Grübler [62]

Table 1. Prior ranges of the model parameters. Lower and upper values are absolute bounds for uniform probability density functions and 95% confidence limits for normal probability density functions.

Parameter	Description	Units	Prior	Lower bound	Upper bound	Reference
a_p	AR coefficient for population growth	dimensionless	uniform	0.85	1	this study[f]
a_g	AR coefficient for GWP growth	dimensionless	uniform	0.85	1	this study[f]
a_c	AR coefficient for carbon emission	dimensionless	uniform	0.85	1	this study[f]
ϵ_p	rms of AR error term for population growth	dimensionless	uniform	0	0.006	this study
ϵ_g	rms of AR error term for GWP growth	dimensionless	uniform	0	0.05	this study
ϵ_c	rms of AR error term for carbon emission	dimensionless	uniform	0	0.09	this study
σ_p	rms of non-annual data for population growth	billions	Jeffreys	0	$+\infty$	Jeffreys [63]
σ_g	rms of non-annual data for GWP growth	Trillion \$/ year	Jeffreys	0	$+\infty$	Jeffreys [63]

Table 2. Prior ranges of **the residual parameters**. Lower and upper values are absolute bounds for uniform probability density functions. "Jeffreys" denotes Jeffreys noninformative prior distribution for the two parameters characterizing the standard deviations of the non-annual data of population and GWP growth.

[a]The lower bound is the peak population in the 0.025% scenario; the upper bound the 2100 population in the 0.975% scenario.

[b]The lower bound is the minimum of the four alternative estimates of Maddison [60] (Table B-1) minus the standard deviation; the upper bound the maximum plus the standard deviation.

[c]The average gross savings rate between 1970 and 2002 according to WRI (2005; `http://earthtrends.wri.org`) is 22% with a standard deviation of 1%. The range given here is the 95% confidence interval, with the standard deviation arbitrarily doubled.

[d]We use the ratio of the 2005 level to the long-term saturation level [22] with a uniform probability density function of $\pm 50\%$.

[e]$A_0 = Q_0^{\lambda/(1+\lambda)}(\delta/s)^{\lambda/(1+\lambda)}(\pi P_0)^{\lambda^2/(1+\lambda)}$. This gives the best estimate for A_0.

[f]The autocorrelation timescale of AR(1) process, which equals is $1/(1-a)$ [64] and characterizes the period of short term business cycle, is $\gtrsim$ 6years [65]. This gives the lower bound of the AR coefficient a. The upper bound of the coefficient is $a \leq 1$ for all AR(1) processes [46, chap. 3].

Figures

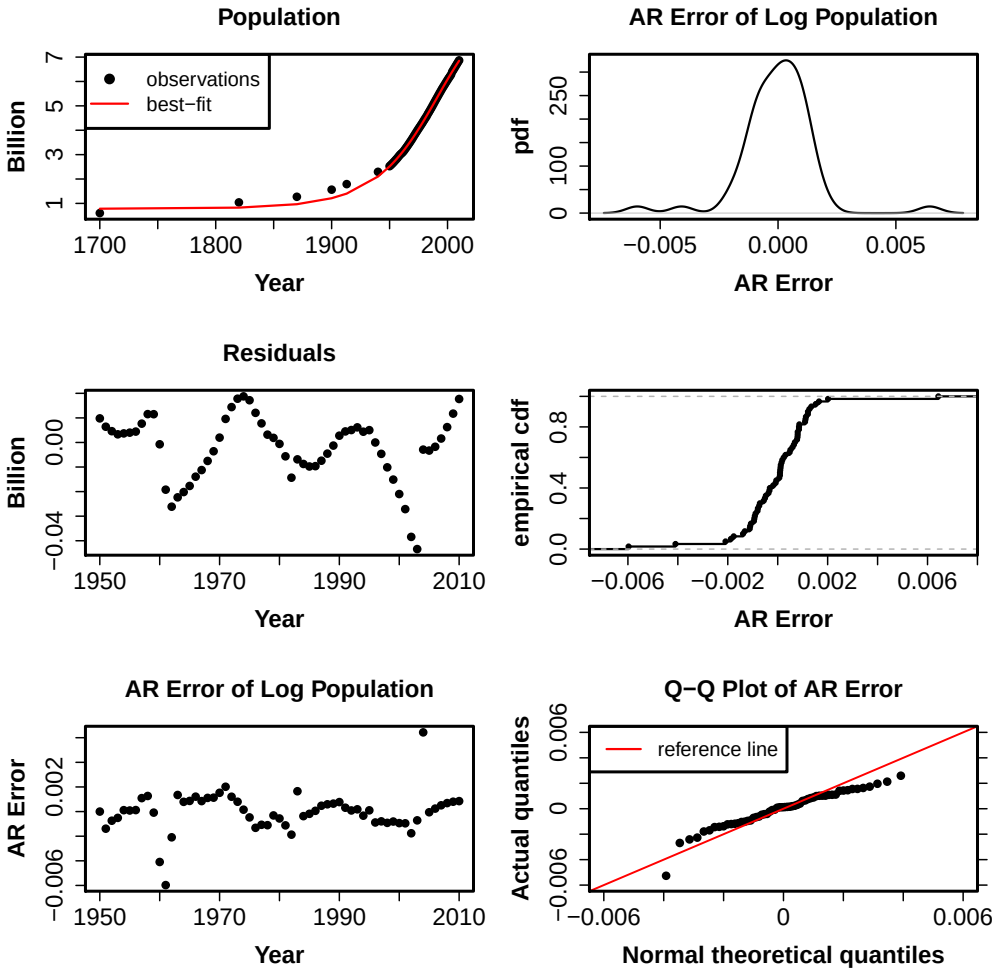

Figure 1. Observations, best-fit model and residuals of the population growth. The left side presents the observations & best-fit model (top-left), residuals of annual data (middle-left), and AR errors of residuals of the annual log population growth (bottom-left). The right side presents probability density function (top-right), cumulative density function (middle-right) and quantile-quantile plot (bottom-right) of the AR errors.

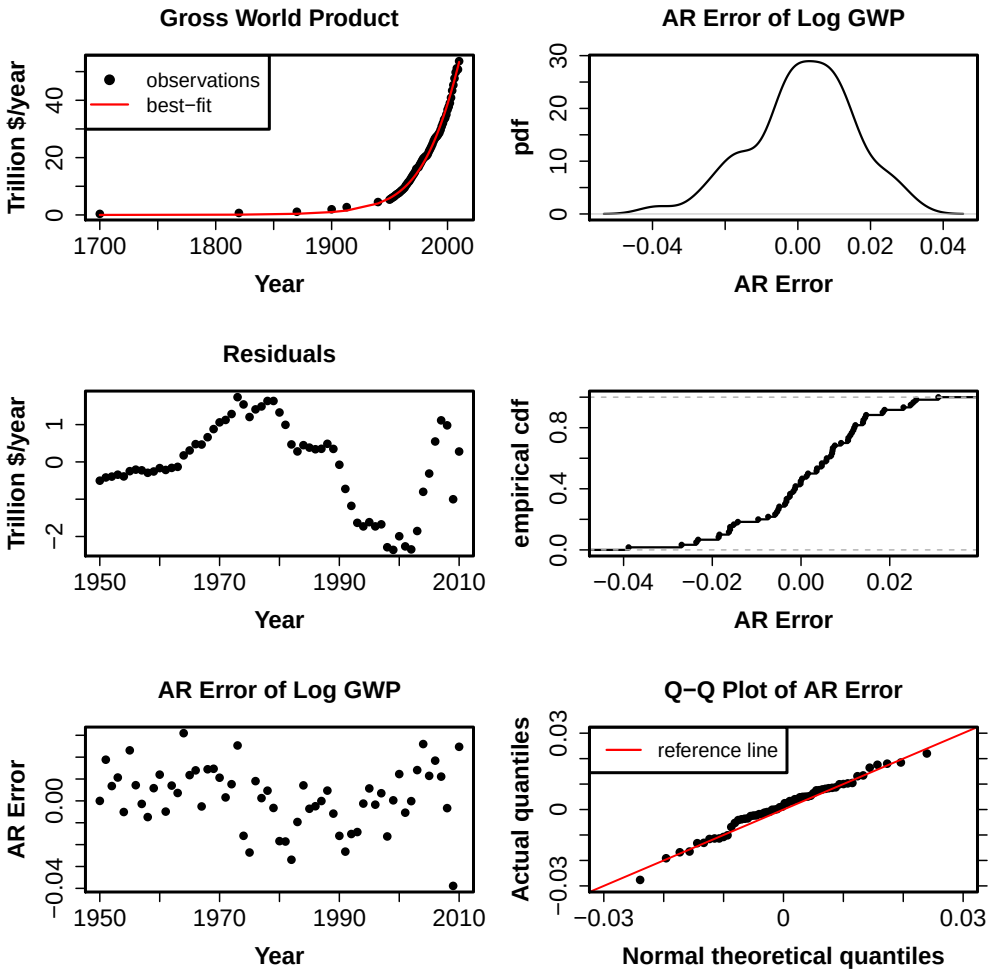

Figure 2. Observations, best-fit model and residuals of the gross world product. The left side presents the observations & best-fit model (top-left), residuals of annual data (middle-left), and AR errors of residuals of the annual log GWP (bottom-left). The right side presents probability density function (top-right), cumulative density function (middle-right) and quantile-quantile plot (bottom-right) of the AR errors.

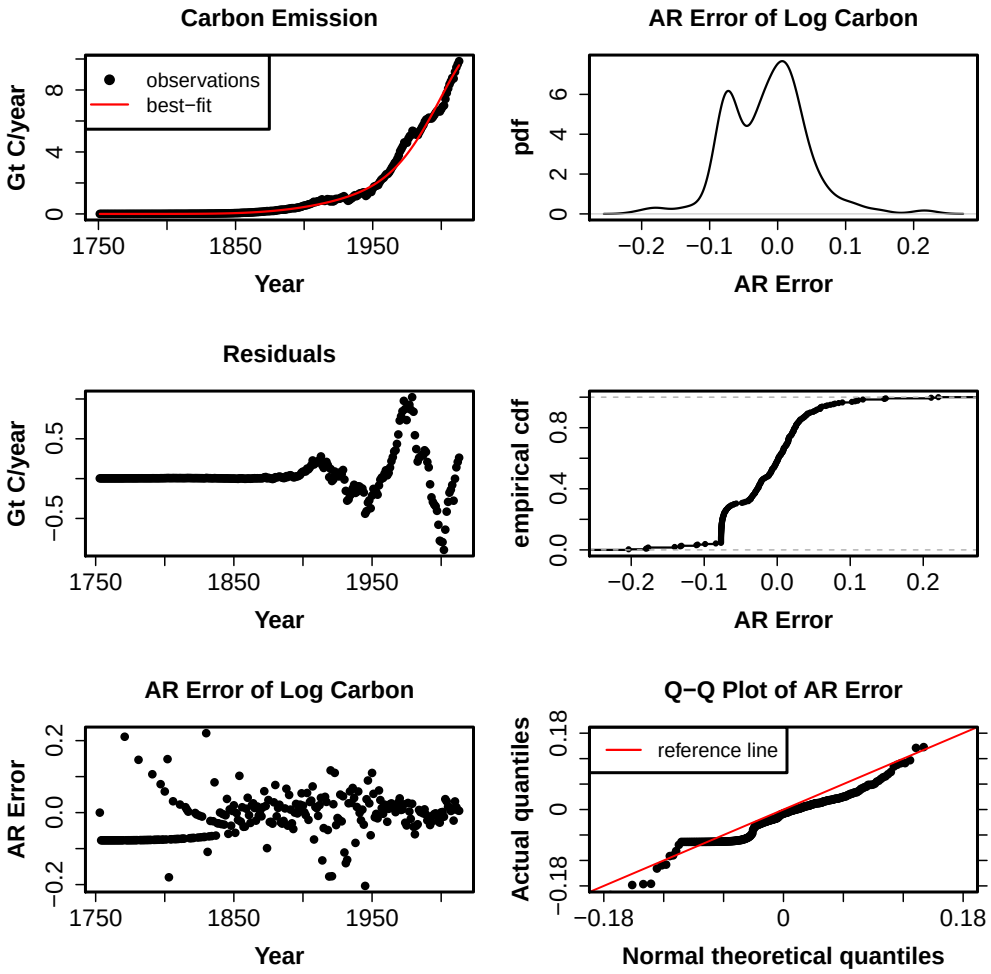

Figure 3. Observations, best-fit model and residuals of the carbon emission. The left side presents the observations & best-fit model (top-left), residuals of annual data (middle-left), and AR errors of residuals of the annual log carbon emission (bottom-left). The right side presents probability density function (top-right), cumulative density function (middle-right) and quantile-quantile plot (bottom-right) of the AR errors.

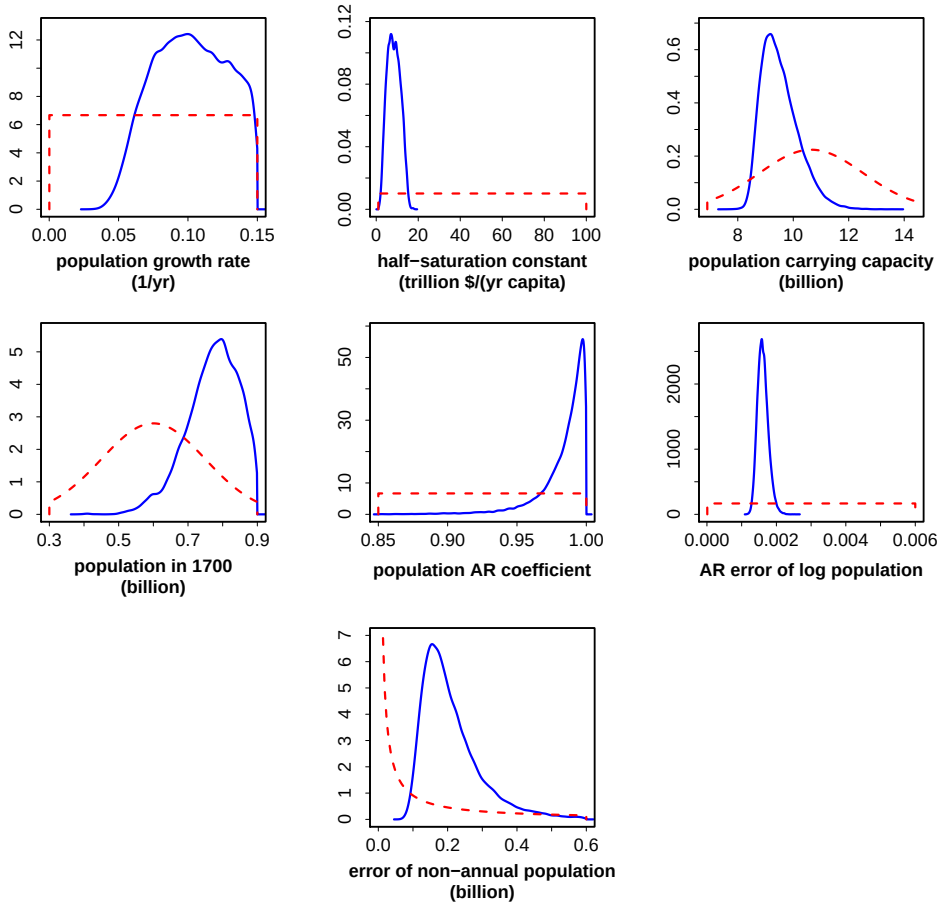

Figure 4. Marginal posteriors of parameters characterizing population growth. The blue solid line denotes posterior and the red dashed line denotes prior.

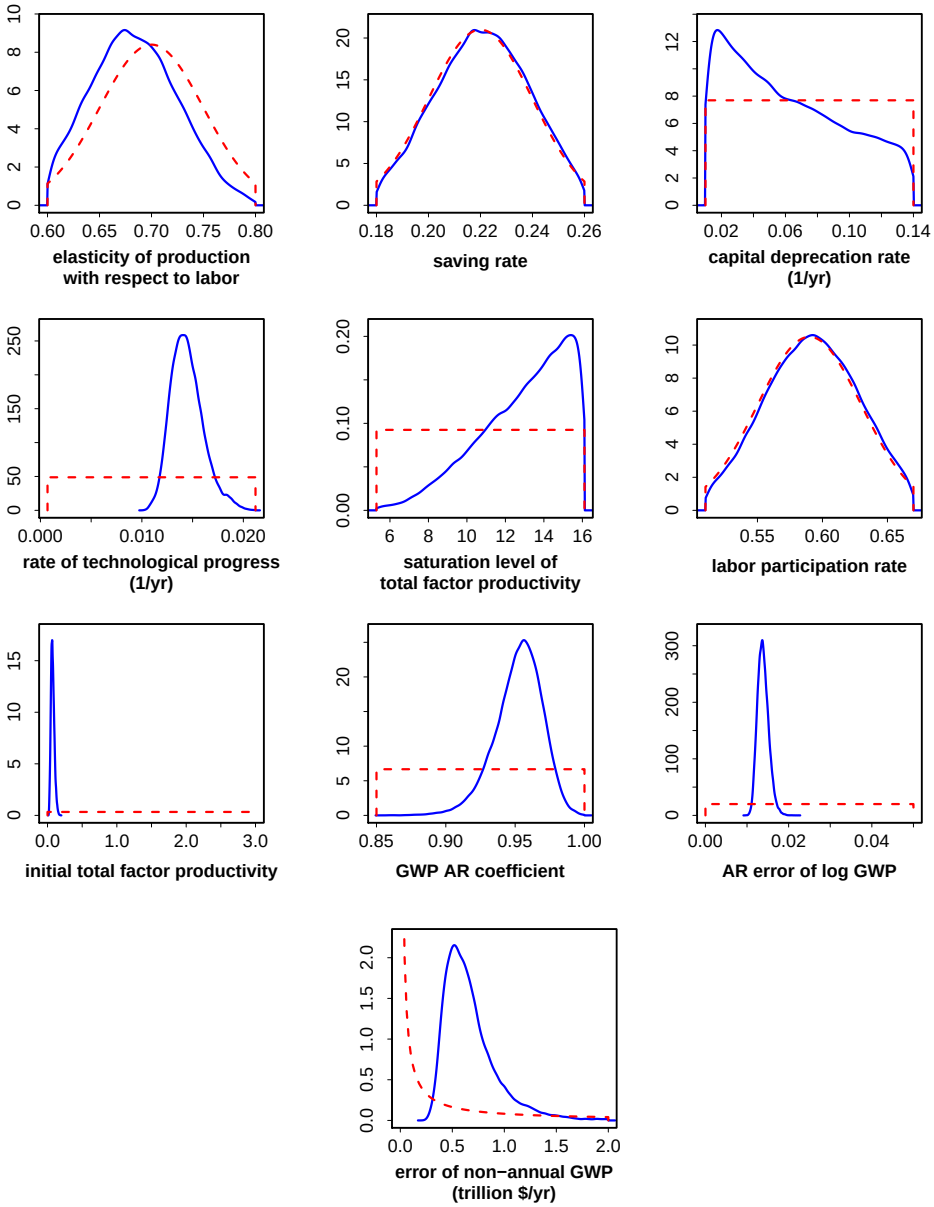

Figure 5. Marginal posteriors of parameters characterizing GWP growth. The blue solid line denotes posterior and the red dashed line denotes prior.

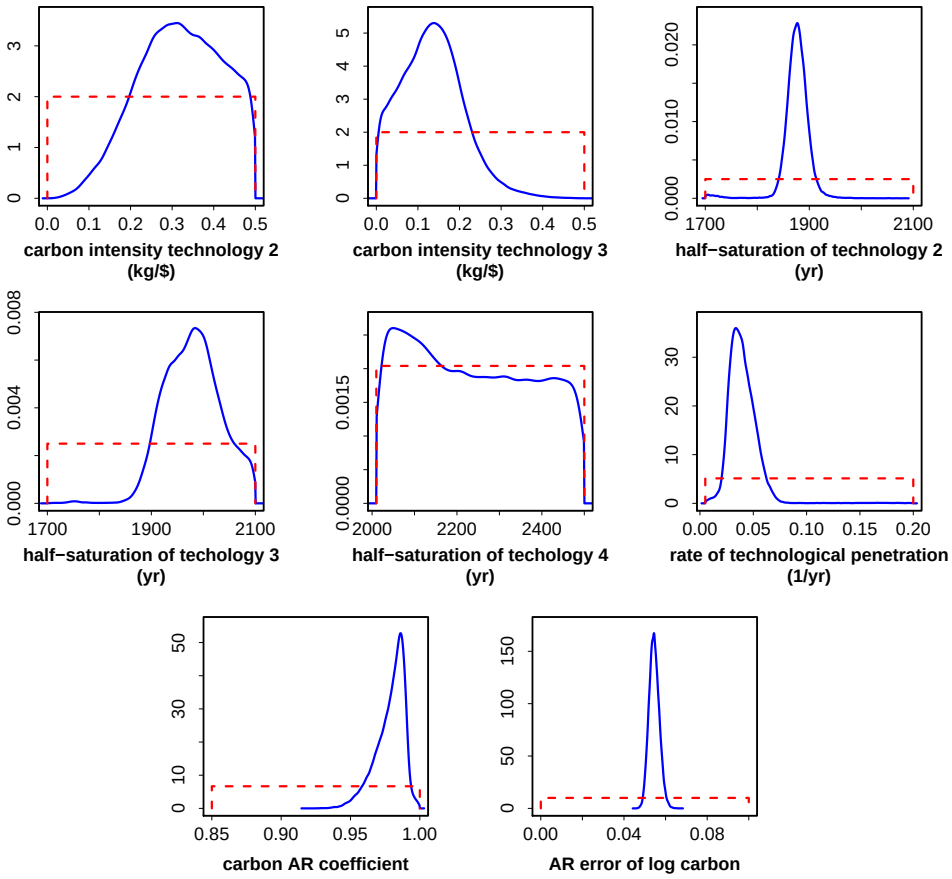

Figure 6. Marginal posteriors of parameters characterizing carbon emission. The blue line denotes posterior and the red dashed line denotes prior.

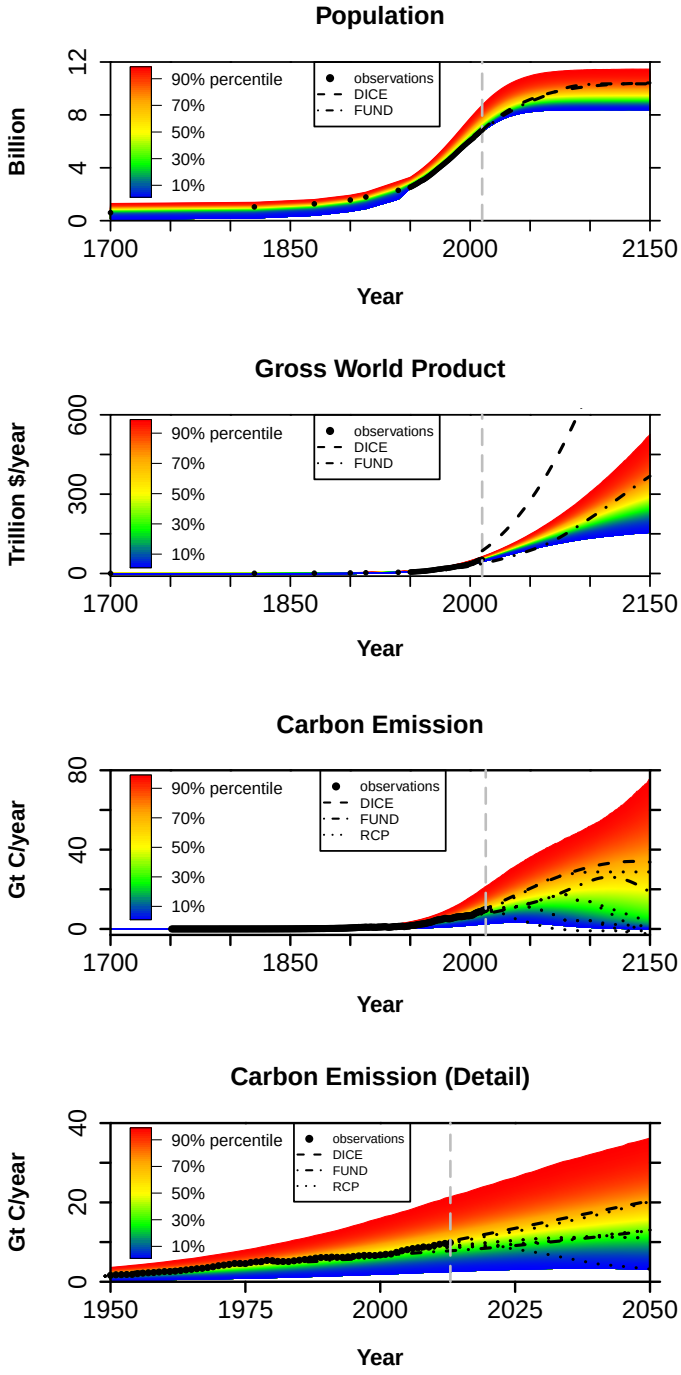

Figure 7. Posterior distributions and posterior predictive distributions of population, GWP and carbon emission from year 1700 to 2150, and their comparison with BAU scenarios of the DICE model, FUND model and RCPs. The 99% percentile range covers all the previous BAU scenarios, except the economic output projection of the DICE model. However, previous BAU scenarios miss important tails of our posterior predictive distributions.

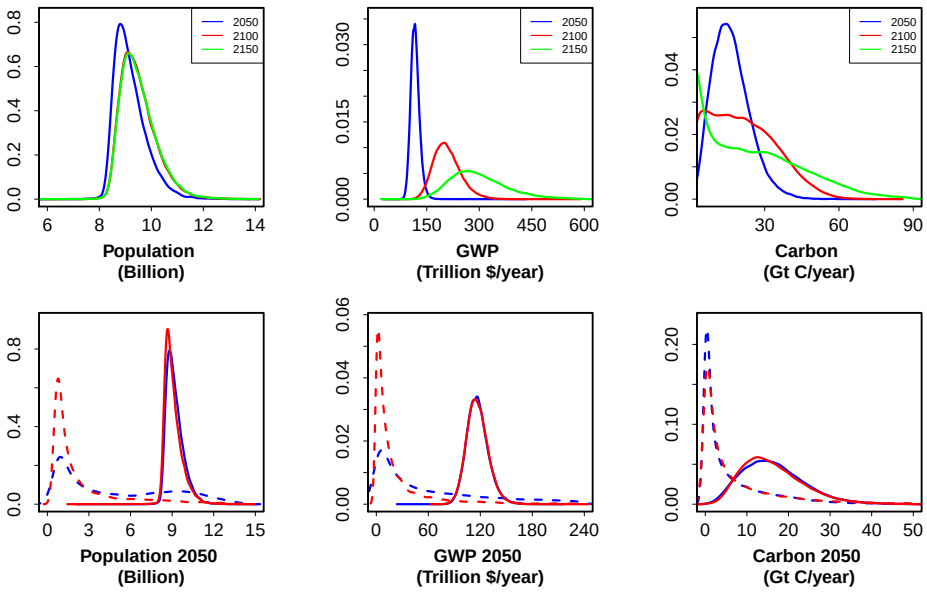

Figure 8. Upper panel: marginal predictive posteriors of population, GWP and carbon emission Projections for the years 2050 (blue line), 2100 (red line) and 2150 (green line). The population level saturates at 9 billion after the year of 2050. The MAP of the GWP gradually grows from about 100 trillion dollars per year at 2050 to about 300 trillion at 2150. The tail of the posterior distribution of the GWP becomes heavier over time. The MAP of the carbon emission decreases from about 15 G t/a to about 0 G t/a. However, the posterior distribution of the carbon emission becomes skewer and has a heavier tail over time. Lower panel: comparison of two different prior predictive distributions and two different posterior predictive distributions of population, GWP and carbon emission at 2050. The blue dash line and blue solid line respectively denote the predictive distributions of first prior and the corresponding posterior. The red dash line and red solid line respectively denote the predictive distributions of the second prior and the corresponding posterior. Although the prior predictive distributions are different for different prior distributions, the posterior predictive distributions converge to the same distributions.